Electron temperature fluctuation measurements with Correlation Electron Cyclotron Emission in L-mode and I-mode plasmas at ASDEX Upgrade

Rachel Bielajew[1,*], *Garrard D* Conway[2], *Tim* Happel[2], *Klara* Höfler[3,2], *Pedro A* Molina Cabrera[4], *Ulrike* Plank[2], *Pablo* Rodriguez-Fernandez[1], *Davide* Silvagni[2], *Branka* Vanovac[1], *Christian* Yoo[1], *Anne* White[1], and The ASDEX Upgrade Team[5]

[1]Plasma Science and Fusion Center, Massachusetts Institute of Technology, Cambridge, MA 02139, USA
[2]Max Plank Institute for Plasma Physics, 85748 Garching, Germany
[3]Department E28, Technical University of Munich, 85748 Garching, Germany
[4]École Polytechnique Fédérale de Lausanne, Swiss Plasma Center, CH-1015 Lausanne, Switzerland
[5]See author list of U. Stroth et al. 2022 Nucl. Fusion **62** 042006

Abstract. The Correlation Electron Cyclotron Emission (CECE) diagnostic at ASDEX Upgrade (AUG) is used to investigate the features of outer core and pedestal (ρ_{pol} = 0.85-1.0) turbulence across confinement regime transitions. The I-mode confinement regime is a promising operational scenario for future fusion reactors because it features high energy confinement without high particle confinement, but the nature of the edge and pedestal turbulence in I-mode plasmas is still under investigation. The edge Weakly Coherent Mode (WCM) appears in the I-mode pedestal and may play a role in transport. In this work we explore electron temperature (T_e) fluctuations in the plasma outer core and pedestal using a 24-channel high radial resolution CECE radiometer. CECE measurements provide turbulence information including the T_e fluctuation amplitude, turbulent spectra, and radial localization of turbulent features. With CECE measurements we show that the WCM is localized in the pedestal region in both L-mode and I-mode and is measured in optically thick plasmas with a T_e fluctuation amplitude of 2.3%. Broadband drift wave turbulence is measured in the outer core with a T_e fluctuation amplitude of <1%. A second CECE system recently installed at AUG allowed for non-standard fluctuation measurements during L-mode and I-mode experiments. The second CECE system was toroidally separated from the primary system, allowing measurements of the long-range toroidal correlation of the WCM indicating its low toroidal mode number. A reflectometer sharing a line of sight with the second CECE system enabled density-temperature cross-phase ($\alpha_{n_eT_e}$) measurements. The WCM $\alpha_{n_eT_e}$ changes between L-mode and I-mode as the T_e gradient steepens.

1 Introduction

Electron temperature (T_e) fluctuation measurements provide important information on plasma confinement scaling and transitions between L-mode and high confinement regimes, as well as the role of edge fluctuations in these regimes. Using the Correlation Electron Cyclotron Emission (CECE) diagnostic at ASDEX Upgrade (AUG), these measurements are obtained with high temporal (4 MHz) and spatial (2 mm) resolution to study turbulence behavior in the high confinement regime I-mode. I-mode is characterized by a heat transport barrier without a particle transport barrier, so it achieves high energy confinement while allowing impurity exhaust and staying below stability boundaries that lead to Edge-Localized Modes (ELMs) [1–3]. I-mode is typically achieved at AUG in the unfavorable ∇B drift configuration because higher heating power can be applied before a transition to ELMy H-mode as compared to the favorable drift configuration.

The nature of turbulence in I-mode and its role in sustaining the I-mode regime is still under investigation, and CECE measurements reveal important properties of the turbulence spanning the region from the outer core (normalized radius $\rho_{pol} < 0.9$) through the pedestal to the last closed flux surface (LCFS) at $\rho_{pol} = 1.0$. The Weakly Coherent Mode (WCM) is a broadband, mid-frequency (40-100 kHz) pedestal fluctuation with a larger density fluctuation amplitude than electron temperature fluctuation amplitude [4, 5]. The WCM has been hypothesized to be important in the transport properties of I-mode, similar to how edge coherent modes in other ELM-free high confinement regimes cause particle transport in place of ELMs (e.g. the Quasi-Coherent Mode in Enhanced D-alpha H-mode and the Edge Harmonic Oscillation in Quiescent H-mode [6, 7]). The WCM has been observed in the density and electron temperature fluctuation signals of AUG L-modes as well [5, 8]. A Low Frequency Edge Oscillation (LFEO) is also observed as a coherent and low-frequency mode in the pedestal of I-modes, and may be a Geodesic Acoustic Mode (GAM) [9]. The GAM is proposed to couple with the WCM and cause its broad structure in frequency space [10, 11].

*e-mail: bielajew@mit.edu

The rest of this paper will present a study of L-modes and I-modes using CECE and coupled diagnostics to probe the nature of the outer core and edge turbulence. In Section 2 we present CECE measurements of T_e fluctuations, which investigate the nature of the WCM and LFEO as well as outer core and pedestal top turbulence. A comparison of favorable and unfavorable drift configuration T_e turbulence is also presented. In Section 3 we present measurements of the WCM using non-standard hardware configurations, including long-range correlation measurements using toroidally separated CECE systems and n_eT_e cross-phase measurements using a coupled reflectometer.

2 CECE measurements

The first CECE diagnostic on AUG shares optics with the 1-D ECE system and has a set of interchangeable radio frequency (RF) sections for tuning measurements to different regions of the plasma. For the following measurements, an RF section with a tunable Gunn oscillator and receiving range of 109-124 GHz was used for edge and pedestal optimized measurements. The RF section sits on a sliding rail so that the antenna beam waist (radius ~7.6 mm) can be moved radially in the plasma. For these measurements the waist was optimized for pedestal measurements. The intermediate frequency (IF) section of the CECE diagnostic features a comb of 24 channels with fixed filters of 200 MHz bandwidth and center frequencies spaced 250 MHz apart. Neighboring CECE channels sit within a turbulence correlation length and measure the same T_e fluctuations but do not share thermal noise. By correlating neighboring channels, coherency spectra (γ_c) of T_e turbulence are obtained. By integrating in frequency space over the turbulent features in the spectra and subtracting the background coherent noise, the normalized fluctuation amplitude ($\delta T_e/T_e$) perpendicular to the magnetic field can be obtained [12].

CECE is used to study T_e turbulence in the outer core through the pedestal region in L-modes and I-modes. Figure 1 shows the T_e fluctuation amplitude over radius during an I-mode phase of a discharge. The fluctuation amplitude rises smoothly from ~ 0.5% in the outer core ($\rho_{pol} < 0.90$) to ~ 1% at the pedestal top ($\rho_{pol} = 0.96$). Then the fluctuation amplitude increases sharply between $\rho_{pol} = 0.97$ and the LCFS due to fluctuations associated with the WCM. At its maximum amplitude at $\rho_{pol} = 0.99$ the WCM fluctuation amplitude is 2.3%. The plasma becomes optically thin ($\tau < 2$) near the LCFS, but the WCM peak amplitude occurs in an optically thick region of the plasma. The fluctuation amplitude over radius gives information about the radial range of the WCM. The WCM fluctuations cover a ρ_{pol} range of ~ 0.02, corresponding to physical width of approximately 1.5 cm. This discharge also had L-mode phases featuring the WCM at the same radial location as in I-mode. There is a reduction in the averaged outer core ($\rho_{pol} < 0.95$) $\delta T_e/T_e$ fluctuation level between L-mode and I-mode from 0.52% to 0.48% but this small change is within error bars.

A spectrogram of T_e fluctuations from a single CECE channel at the WCM peak at $\rho_{pol} = 0.99$ is shown in Fig-

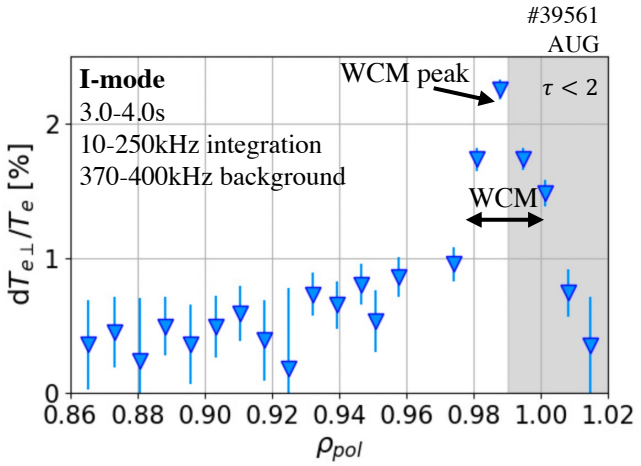

Figure 1. Electron temperature fluctuation level over radius for an I-mode phase of a discharge. The turbulence integration window was 10-250 kHz and the background subtraction window was 370-400 kHz in the calculation of fluctuation amplitude. The region of marginal optical depth $\tau < 2$ are shaded in grey. Fluctuation levels rise from ~ 0.5% in the outer core to 2.3% at the WCM peak near $\rho_{pol} = 0.99$.

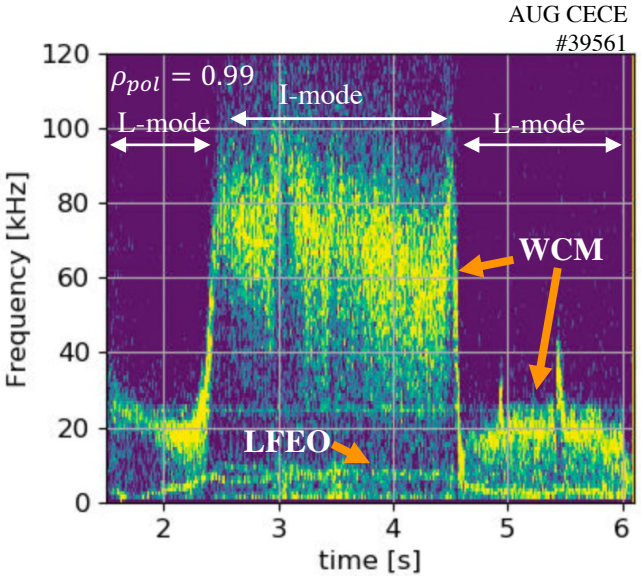

Figure 2. Spectrogram from CECE channel 19 near the WCM peak amplitude of $\rho_{pol} = 0.99$. The discharge develops from L-mode (<2.4s) to I-mode (2.4-4.5s) to L-mode (>4.5s) and the WCM appears as the 20 kHz mode in L-mode which spins up to the 40-90 kHz in I-mode, and then back to 20 kHz in L-mode. LFEO is the narrowband mode at 8 kHz which appears in the I-mode phase only.

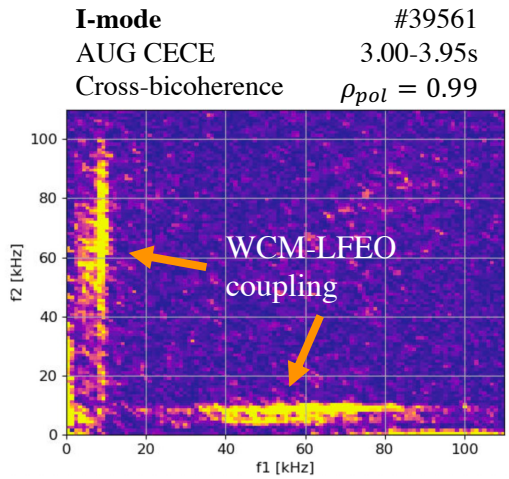

Figure 3. Cross-bicoherence of neighboring CECE channels near the WCM peak location of $\rho_{pol} = 0.99$. Coupling is seen between the WCM (40-80 kHz) and the LFEO (8 kHz). FFT bins of 4096 were used for the analysis with 1855 overlapping ensembles.

ure 2. This discharge develops from L-mode (<2.4s) to I-mode (2.4-4.5s) then back to L-mode (>4.5s). The WCM appears as the 20 kHz mode in L-mode which spins up to the 40-90 kHz in I-mode, and then back to 20 kHz in L-mode. The frequency shift between L-mode and I-mode may correspond with a change of radial electric field between L-mode and I-mode and the Doppler shift of fluctuations due to increased $E \times B$ velocity. The LFEO can also be seen during the I-mode phase of the discharge as the coherent mode at $\sim$ 8 kHz.

The WCM and LFEO are coupled as seen in Figure 3, which shows the cross-bicoherence between neighboring CECE channels near the WCM location of $\rho_{pol} = 0.99$. The analysis shows that the the narrow-band LFEO at 8 kHz is coupled with the broadband WCM at 40-90 kHz.

In addition to the L-mode/I-mode comparison, L-mode phases were compared in matched favorable and unfavorable ∇B drift configuration discharges. Figure 4 shows the CECE coherency spectra at the pedestal top ($\rho_{pol} = 0.96$) and the WCM location ($\rho_{pol} = 0.99$) during three ECRH power steps. Both the favorable and unfavorable configuration discharges are in L-mode for the first two power step (0.2 MW and 0.6 MW) and in these phases discharge parameters including temperature and density are matched. During the lowest power step, there is very little difference in the turbulence at the pedestal top between the favorable and unfavorable configuration discharges (Fig. 4a). During this low power step, the beginnings of the formation of the WCM can be seen at $\rho_{pol} = 0.99$ in both the favorable and unfavorable configurations as the broadband mode centered around 30 kHz (Fig. 4d). The WCM-like feature is stronger (a higher value of $|\gamma_c|$) in the unfavorable configuration as compared to the favorable configuration. During the second power step, at the pedestal top the fluctuations in the unfavorable configuration are slightly stronger than the fluctuations in the favorable configuration (Fig. 4b). At the WCM location, in unfavorable configuration the WCM feature appears more strongly than at lower power. In favorable configuration the WCM is no longer visible as a distinct broadband mode (Fig. 4e). At the highest power step, the unfavorable configuration discharge remains in L-mode and the fluctuations at the pedestal top are still visible in the coherency spectra (Fig. 4c) while the WCM is clearly visible in the spectra at $\rho_{pol} = 0.99$ (Fig. 4f). The favorable configuration discharge has transitioned to ELMy H-mode, so the plasma parameters no longer match with the unfavorable configuration discharge and the fluctuations are mostly beneath the sensitivity limit at both the pedestal top and $\rho_{pol} = 0.99$. Whether the disappearance of the WCM is a result of $E \times B$ shear remains to be investigated.

3 CECE diagnostic extension measurements

In addition to the standard CECE analysis presented using the 24-channel comb, nonstandard measurements were taken using a second CECE system and a coupled reflectometer to investigate additional physics of the WCM.

3.1 Long-range correlations

A second CECE system was installed at AUG at a second port which was toroidally separated by 60° from the primary CECE system. As with the primary system, the new CECE system also features a 24-channel comb with IF filters of 200 MHz bandwidth with centers spaced apart by 250 MHz. The RF front ends are interchangeable, and for these experiments the diagnostic was optimized for edge measurements with a receiving range of 105-113 GHz. This CECE diagnostic was installed on the same oversized waveguide as the Doppler Reflectometers and shares their antenna and focusing mirror.

The secondary CECE system was operated during the L-mode/I-mode discharge previously presented. The safety factor during this discharge at $\rho_{pol} = 0.99$ and the toroidal separation between the two CECE systems place the edge CECE channels in the two systems on approximately the same magnetic field line. The correlation between CECE channels near the WCM location ($\rho_{pol} = 0.99$) is shown in Figure 5, as the γ_c spectra between these toroidally separated channels. The standard CECE γ_c spectra of two neighboring channels in the same radial comb is overlaid with normalized amplitude for comparison. Both the WCM and LFEO are clearly visible in the long-range correlations. This toroidal correlation indicates that the both the WCM and LFEO have low toroidal mode number.

3.2 $n_e T_e$ cross-phase measurements

The phase between density and temperature fluctuations, $\alpha_{n_e T_e}$, has previously been used to quantify the mixture of ion temperature gradient (ITG) versus trapped electron

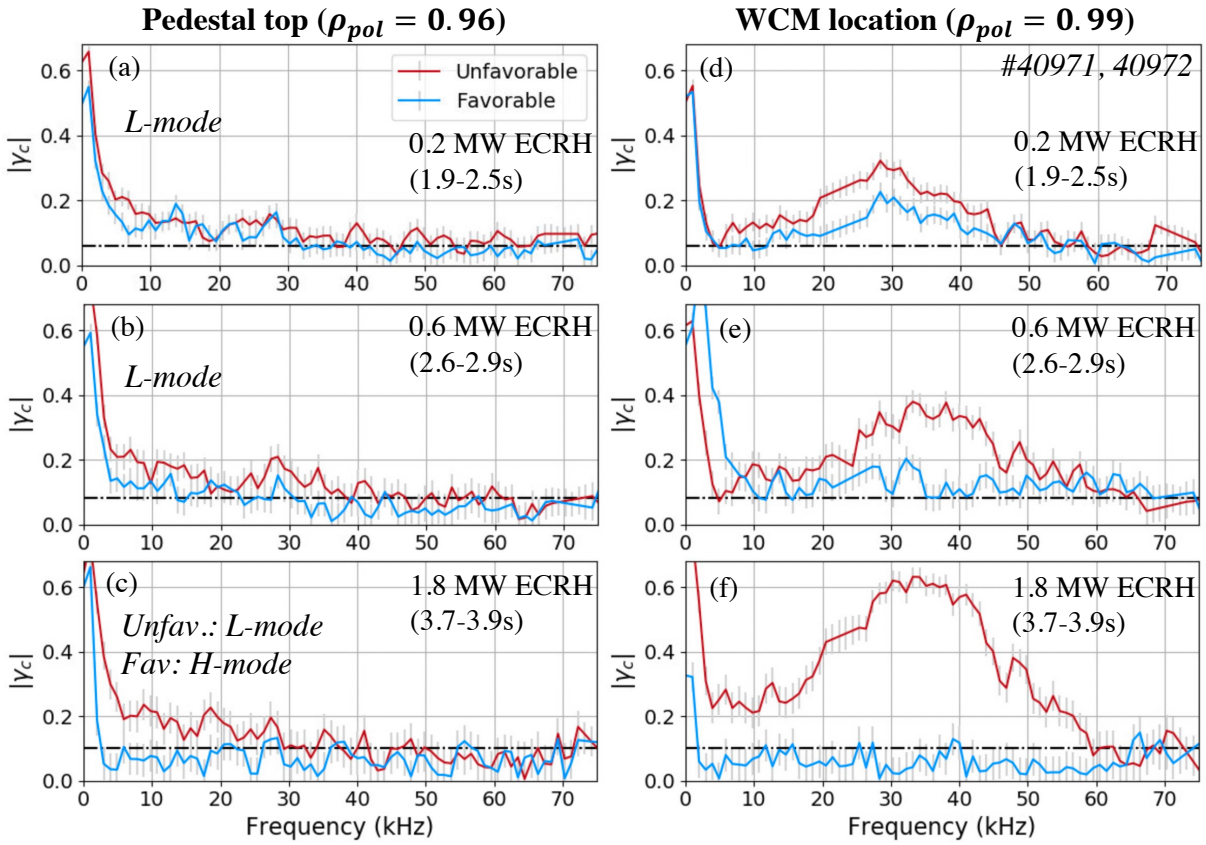

Figure 4. CECE coherency spectra in matched favorable (blue, 40972) and unfavorable (red, 40971) configuration discharge phases. Pedestal top (a-c) and the WCM location (d-f) are shown at three different ECRH power steps: 0.2 MW (a, d), 0.6 MW (b,e), and 1.8 MW (c,f). The unfavorable configuration plasma remains in L-mode for all power steps while the favorable configuration is in H-mode at the highest power step. WCM formation can be seen in all power steps in unfavorable configuration, and only the lowest power step in favorable configuration.

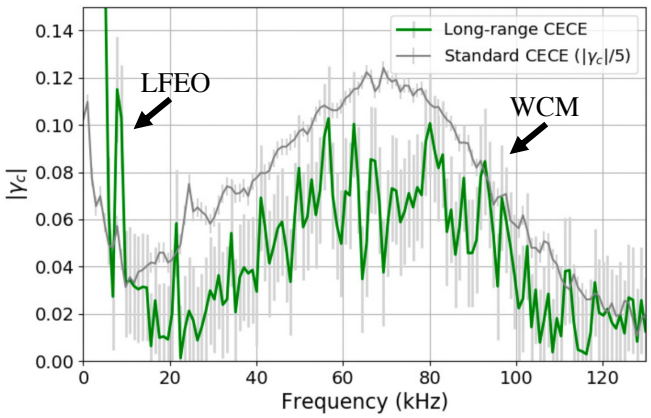

Figure 5. CECE coherency spectra obtained by correlating channels near the WCM location at $\rho_{pol} = 0.99$ from CECE systems toroidally separated by ~60° (green). CECE coherency spectra from standard CECE analysis with neighboring channels in a single system is overlaid in grey, with a normalization factor for clear visualization. The WCM is visible in both the long-range and local correlations.

mode (TEM) turubulence in core plasmas, and as a metric for validating gyrokinetic codes [13–15]. This measurement provides valuable information about the nature of the plasma turbulence. The n_eT_e phase diagnostic was operated during the L-mode/I-mode experiments by coupling the secondary CECE system and the Doppler Reflectometers in this sector of the tokamak using a 3dB wire-grid splitter and the same data acquisition system for both CECE and reflectometer signals. If radial alignment between the CECE channels and the reflectometer cutoff is achieved via appropriate choice of reflectometer frequency then $\alpha_{n_eT_e}$ may be obtained from the correlation between the reflectometer and CECE signals.

The $\alpha_{n_eT_e}$ analysis is shown in Figure 6 during the L-mode and I-mode phases of the discharge. There is coherency between the reflectometer and the CECE channel in the WCM range of frequencies in both L-mode and I-mode, as shown by Fig. 6a and c. From these correlations, $\alpha_{n_eT_e}$ is extracted and shown in degrees in Fig. 6b and d. Over the range of frequencies where there is coherency between the reflectometer and CECE signals, there is an evident, out-of-phase n_eT_e cross phase in both L-mode and I-mode. The L-mode WCM cross phase is farther out-of-phase than the I-mode WCM, with $\alpha_{n_eT_e} = -171°$ at the peak CECE-reflectometer in L-mode as compared

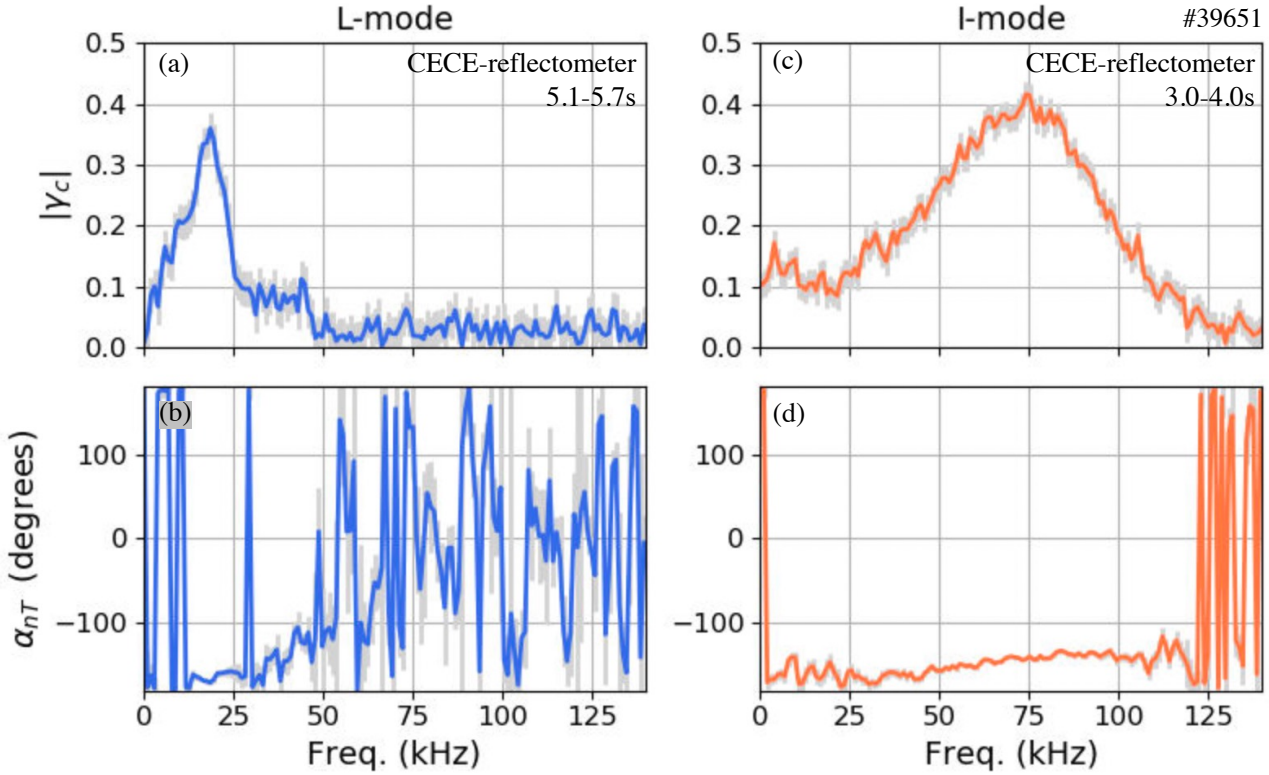

Figure 6. Coherency between a CECE channel and V-band reflectometer at $\rho_{pol} = 0.98$ during (a) L-mode and (c) I-mode phases, showing the WCM at 20 kHz in L-mode and 40-100 kHz in I-mode. The n_eT_e phase over frequency obtained from CECE-reflectometer correlations shown in (b) L-mode and (d) I-mode. The n_eT_e phase at the spectral peak of the WCM is $-171°$ in L-mode and shifts to $-143°$ in I-mode.

to $-143°$ at the peak coherency in I-mode. This change from out-of-phase to less out-of-phase between L-mode and I-mode occurs as ∇T_e steepens between L-mode and I-mode, so is consistent with previous measurements and simulations that have shown $\alpha_{n_eT_e}$ to change with ∇T_e due to increased TEM drive [13, 15]. However, the WCM $\alpha_{n_eT_e}$ values observed here are farther out-of-phase than previous core turbulence $\alpha_{n_eT_e}$ measurements, indicating that the WCM may be of a different nature than core turbulence. The n_eT_e cross-phase does not enter directly into cross-field heat and particle transport equations. Therefore, these measured $\alpha_{n_eT_e}$ values alone do not give information about the direction of heat versus particle transport for the WCM without further assumptions about the $n_e\phi$ cross-phase, the relationship between $n_e\phi$, $T_e\phi$, and n_eT_e cross-phases, the n_e to T_e fluctuation amplitude ratio, as well as assuming the WCM to be electrostatic in nature.

The slope of $\alpha_{n_eT_e}$ over the frequency range of CECE-reflectometer coherency can provide information about the poloidal velocity of the WCM. Because of a small poloidal separation between the reflectometer and CECE, there is a finite time delay between the WCM's appearance across the reflectometer cutoff and the CECE resonance, which corresponds to a change in $\alpha_{n_eT_e}$ with frequency. The I-mode WCM $\alpha_{n_eT_e}$ has a change of approximately 25° over a frequency range of 60 kHz, which corresponds to a time delay of 1.2 μs. The CECE channel and reflectometer are separated by approximately 4 mm. This corresponds to a poloidal velocity of approximately 3 km/s, which is similar to previously reported values at the L-mode and I-mode WCM location [8]. This estimation is performed in the laboratory frame, and the background plasma velocity would be needed to calculate the WCM's phase velocity in the plasma frame. The L-mode WCM is too narrowband to determine if $\alpha_{n_eT_e}$ has a slope over its frequency range.

The out-of-phase $\alpha_{n_eT_e}$ measurements also have implications for quantifying the effect of n_e fluctuations on the radiated temperature signals collected by CECE as the optical depth becomes marginal ($\tau < 2$) near the LCFS. In L-mode phases, the WCM peak often occurs in this marginal region with $1 < \tau < 2$. Following the analysis of Reference [16], the I-mode $\alpha_{n_eT_e}$ values which are neither in-phase nor completely out-of-phase suggests that the CECE measurements of the WCM are robustly T_e fluctuations with little impact from n_e fluctuations. The L-mode $\alpha_{n_eT_e}$ is close to completely out-of-phase, which indicates that n_e fluctuations may cause the apparent radiated temperature fluctuation amplitude to be less than the actual T_e fluctuation amplitude at the L-mode WCM location.

4 Conclusions

A 24-channel high radial and time resolution CECE system was used to study outer core and pedestal turbulence in L-modes and I-modes at AUG. The characteristic I-mode fluctuations of the WCM and the LFEO are both

visible in CECE spectra and these two modes are shown to be coupled by bicoherence analysis. Radial profiles of the T_e fluctuation amplitude shows that turbulence increases from $\sim$ 0.5% in the outer core to $\sim$ 1% at the pedestal top. Then, the T_e fluctuation amplitude increases sharply due to the localized WCM fluctuations ($\rho_{pol} = 0.98 - 1.0$), with a peak around $\rho_{pol} = 0.99$ where $\delta T_e/T_e = 2.3\%$. The WCM is also present in L-mode as a more coherent mode at lower frequency than in I-mode. An investigation of turbulence was performed in matched favorable and unfavorable ∇B drift configuration L-mode plasmas. CECE coherency spectra show that the WCM is present in both favorable and unfavorable configurations at low heating power, but at slightly higher heating power in unfavorable configuration the WCM is strengthened while in favorable configuration the WCM is no longer visible. At low power, the outer core fluctuations are matched in favorable and unfavorable configurations, while at higher power the unfavorable configuration has stronger fluctuations than the favorable configuration.

Non-standard CECE diagnostic extensions allowed for a deeper investigation of the physics of the edge fluctuations in L-modes and I-modes. Long-range correlations performed across toroidally separated CECE systems showed that both the WCM and the LFEO are correlated over long toroidal distances and therefore have low toroidal mode numbers. The coupled reflectometer-CECE system allowed for $\alpha_{n_eT_e}$ measurements which provide valuable information about the nature of the WCM including how it changes between L-mode and I-mode with ∇T_e and its poloidal velocity. The value of $\alpha_{n_eT_e}$ alone cannot be used to determine the direction particle versus heat transport from the WCM. These cross-phase measurements in conjunction with optical depth calculations can also assist in quantifying the impact of n_e fluctuations on the radiated temperature fluctuation signals.

5 Acknowledgements

This work has been carried out within the framework of the EUROfusion Consortium, and has received funding from the Euratom Research and Training Programme (Grant Agreement No 101052200 — EUROfusion). The views and opinions expressed herein do not necessarily reflect those of the European Commission. This work was also supported by the US Department of Energy under grants DE-SC0014264, DE-SC0006419, and DE-SC0017381.

References

[1] D.G. Whyte, A.E. Hubbard, J.W. Hughes, B. Lipschultz, J.E. Rice, E.S. Marmar, M. Greenwald, I. Cziegler, A. Dominguez, T. Golfinopoulos et al., Nuclear Fusion **50**, 105005 (2010)

[2] T. Happel, P. Manz, F. Ryter, P. Hennequin, A. Hetzenecker, G.D. Conway, L. Guimarais, C. Honoré, U. Stroth, E. Viezzer, Nuclear Fusion **56** 064004 (2016)

[3] D. Silvagni, T. Eich, T. Happel, G.F. Harrer, M. Griener, M. Dunne, M. Cavedon, M. Faitsch, L. Gil, D. Nille et al., Nuclear Fusion **60** 126028 (2020)

[4] A.E. White, P. Phillips, D.G. Whyte, A.E. Hubbard, C. Sung, J.W. Hughes, A. Dominguez, J. Terry, I. Cziegler, Nuclear Fusion **51** 113005 (2011)

[5] T. Happel, M. Griener, D. Silvagni, S.J. Freethy, P. Hennequin, F. Janky, P. Manz, D. Prisiazhniuk, F. Ryter, M. Bernert et al., Nuclear Materials and Energy **18** 159-165 (2019)

[6] A.E. Hubbard, R.L. Boivin, R.S. Granetz, M.Greenwald, J.W. Hughes, I.H. Hutchinson, J. Irby, B. LaBombard, Y. Lin, E.S. Marmar et al., Physics of Plasmas **8** 2033 (2001)

[7] K.H. Burrell, W.P. West, E.J. Doyle, M.E. Austin, T.A. Casper, P. Gohil, C.M. Greenfield, R.J. Groebner, A.W. Hyatt, R.J. Jayakumar et al., Physics of Plasmas **12** 056121 (2005)

[8] R. Bielajew, G.D. Conway, M. Griener, T. Happel, K. Höfler, N.T. Howard, A.E. Hubbard, W. McCarthy, P.A. Molina Cabrera, T. Nishizawa et al., Physics of Plasmas **29** 052504 (2022)

[9] W. McCarthy Ph.D. Thesis, Massachusetts Institute of Technology Cambridge, MA (2022)

[10] I. Cziegler, P.H. Diamond, N. Fedorczak, P. Manz, G.R. Tynan, M. Xu, R.M. Churchill, A.E. Hubbard, B. Lipschultz, J.M. Sierchio et al., Physics of Plasmas **20** 055904 (2013)

[11] P. Manz, P. Lauber, V.E. Nikolaeva, T. Happel, F. Ryter, G. Birkenmeier, A. Bogomolov, G.D. Conway, M.E. Manso, M. Maraschek et al., Nuclear Fusion **55** 83004 (2015)

[12] A.J. Creely, S.J. Freethy, W.M. Burke, G.D. Conway, R. Leccacorvi, W.C. Parkin, D.R. Terry, A.E. White, Review of Scientific Instruments **89** 53503 (2018)

[13] J.C. Hillesheim, J.C. DeBoo, W.A. Peebles, T.A. Carter, G. Wang, T.L. Rhodes, L. Schmitz, G.R. McKee, Z. Yan, G.M. Staebler et al., Physics of Plasmas **20** 056115 (2013)

[14] A.E. White, W.A. Peebles, T.L. Rhodes, C.H. Holland, G. Wang, L. Schmitz, T.A. Carter, J.C. Hillesheim, E.J. Doyle, L. Zeng et al., Physics of Plasmas **17** 056103 (2010)

[15] S.J. Freethy, T. Görler, A.J. Creely, G.D. Conway, S.S. Denk, T. Happel, C. Koenen, P. Hennequin, A. E. White, Physics of Plasmas **25** 055903 (2018)

[16] T.D. Rempel, R.F. Gandy, A.J. Wootton, Review of Scientific Instruments, **65**, 2044-2048 (1994)